sciendo Applied Mathematics and Nonlinear Sciences, 9(1) (2024) 1-17

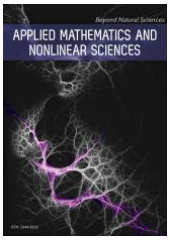

Applied Mathematics and Nonlinear Sciences

https://www.sciendo.com

Optimal seismic solution design for underground frame structure of subway station considering uniform damage

Hongshuo Sun[1,†], Hongtao Dai[1]

1. College of Railway Engineering, Zhengzhou Railway Vocational and Technical College, Zhengzhou, Henan, 451460, China.

Submission Info

Communicated by Z. Sabir
Received January 13, 2023
Accepted April 25, 2023
Available online October 15, 2023

Abstract

Based on the dynamic finite element theory, this paper establishes a fully coupled Mohr-Coulomb plastic finite element model of the soil ontology with the A metro station structure as the research object, conducts a nonlinear dynamic response analysis of the model structure, studies the variation of the seismic response of the model under different vibrations, soil material parameters and concrete parameters, and analyzes the influence of the station structure form on the displacement. In EL-2 condition, the first pair displacement of the S3 measurement point of the rectangular station is 5.695 mm, and the displacement of the arch-shaped station is 2.5 mm less than that of the rectangular station. The relative displacement of soil shear modulus with Gmax=200 MPa is 2.3 mm less than that of soil shear modulus with Gmax=80 MPa in the case of sidewall height of 3 m, which indicates that both the shape of station and soil stiffness has an effect on the seismic performance of the station. Influence on the seismic performance of the station. The research in this paper has an important reference value for the seismic design of underground frames of subway stations.

Keywords: Finite element model; Dynamic response; Uniform damage; Nonlinear analysis; Seismic performance.
AMS 2010 codes: 65D17

†Corresponding author.
Email address: 11082@zzrvtc.edu.cn

ISSN 2444-8656
https://doi.org/10.2478/amns.2023.2.00626

1 Introduction

The subway station complex is moving from a single transportation station to an urban transportation hub complex that integrates transportation, commercial, residential, and entertainment functions [1-2]. As an emerging architectural element introduced by cities in recent years, metro stations can be metro station complexes that can come to drive the development of surrounding plots, thus accelerating urban economic development and social activities [3-4]. Urban underground structures are an important part of urban functions, and urban underground structures are characterized by complex structural forms, large spatial scales, safety hazards that are not easy to detect and difficult to repair, and are crucial for maintaining their safety and functions when strong earthquakes come [5-6]. Although subway stations as underground structures have better seismic performance than surface buildings, these structures are difficult to repair once damage occurs [7-8]. Moreover, damage to subway stations can also cause damage to above-ground buildings and facilities, resulting in chain damage leading to major safety accidents [9-10].

Nowadays, the seismic study of subway station complexes is particularly important as more complex structures and involves many factors such as economic effects and human mobility [11]. The seismic response of the subway station complex structure is not only related to its own structural properties but also involves the dynamic interaction between the subway station-soil-adjacent underground structures [12-13].

Miao et al. used the finite element software ABAQUS to develop a fully coupled model of the soil-structure interaction system and analyzed the damage to the subway structure by different seismic waves [14]. The effect of the central column of a subway station on the seismic performance of the station was studied by Hou et al., and the results of his data support the idea that increasing the aspect ratio of the columns can improve the seismic performance of the station [15]. Xu et al. studied the nonlinear dynamic interaction of soil with subsurface structures in liquefied foundations and suggested that soil liquefaction attenuates the seismic performance of stations [16]. Liang et al. compared the differences in seismic response of subway stations between linear and nonlinear soils and between water-saturated and dry soils and suggested that the nonlinear and water-saturated soil states of soils have a direct impact on the seismic performance of subways [17]. Chen et al. proposed that the deeper the structure is buried, the better the seismic performance of the subway station and that the soft soil structure has a weakening effect on the seismic resistance of the subway [18].

In this paper, we first study the process of implementing dynamic finite element analysis, discretize the structural solution domain, perform unit analysis and construct interpolation functions to construct the system dynamic equilibrium equations, and use the implicit Newmark method to solve the dynamic equilibrium equations. Then, based on the finite element theory, the structure of the subway station is modeled, the Mohr-Coulomb plasticity model of the soil ontology is established, and the plastic damage of concrete and the stress-strain relationship curve of concrete are analyzed by this model. Finally, the seismic performance of the underground frame structure of the subway station is analyzed, and the influence of the concrete strength and soil stiffness on the seismic performance of the underground frame structure of the station is investigated under different operating conditions.

2 Dynamic finite element analysis

2.1 Dynamic finite element

The finite element method is currently the most effective SUSI analysis method. In the dynamic analysis of a structure using the finite element method, the action of the external load on the structure

is always a function of time, and the function needs to be solved from the beginning of the input of the external load to the end of the process, so as to obtain the internal force and deformation of the structure at any moment. The basic idea of the dynamic finite element method is to discretize the solution domain of a structure or a continuum into several discrete units, and these discrete units are ordered in some form to form an aggregate instead of the original structure or continuum.

The following are the steps of the dynamic finite element solution.

1) Discretize the structure solution domain.

2) Perform unit analysis and construct interpolation functions.

3) Construct the system dynamic equilibrium equation.

4) Introduce the boundary conditions.

5) Solve the dynamic equations.

2.2 Establishment of the dynamic equilibrium equation

Physical force per unit volume of moving object:

$$\{p\} = \{p_s\} - \rho \frac{\partial^2}{\partial t^2}\{\delta\} - v\frac{\partial}{\partial t}\{\delta\} \tag{1}$$

Where ρ is the material density, v is the damping factor, $\{p\}$ is the gravitational and other static forces, $\{\delta\}$ is the motion displacement, $\rho \frac{\partial^2}{\partial t^2}\{\delta\}$ is the inertia force, and $v\frac{\partial}{\partial t}\{\delta\}$ is the damping force.

When the finite element method solves for the displacement, the displacement takes the form of:

$$\{f\} = [N]\{\delta\}^e n \tag{2}$$

Where $[N]$ is the form function matrix and $\{\delta\}^e$ is the unit node displacement matrix.

The unit damping matrix, mass matrix, and stiffness matrix are:

$$\begin{cases} \left[C^e\right] = \int [N]^T U [N] dV \\ \left[M^e\right] = \int [N]^T \rho [N] dV \\ \left[K^e\right] = \int [B]^T [D][B] dV \end{cases} \tag{3}$$

The dynamic equilibrium equation for the soil-subsurface structure interaction:

$$[M]\{\ddot{\delta}\} + [C]\{\dot{\delta}\} + [K]\{\delta\} = -[M]\left\{\ddot{\delta}_g\right\} \tag{4}$$

2.3 Solution of the dynamic equilibrium equation

In solving SSI problems using the finite element method, there are usually two methods, showing the central difference method, and the implicit Newmark method. In this paper, the implicit Newmark method is used to solve the dynamic equilibrium equation, which is more suitable for analyzing a series of nonlinear dynamic problems. Its analytical principle is as follows.

1) Initial operations

Generate the damping matrix, mass matrix, and stiffness matrix: $[C]$, $[M]$, $[K]$.

Calculate the initial acceleration, velocity, and displacement vectors: $\ddot{\delta}_0$, $\dot{\delta}_0$, δ_0.

Select time step ${}_{\Delta}t$, parameters α and δ integration constants:

$$\delta \geq 0.50 \quad \alpha = 0.25(0.5+\delta)^2 \tag{5}$$

$$\alpha_0 = \frac{1}{\alpha_{\Delta t} 2}, \alpha_1 = \frac{\delta}{\alpha_{\Delta t}}, \alpha_2 = \frac{1}{\alpha_{\Delta} t}, \alpha_3 = \frac{1}{2\alpha} - 1, \tag{6}$$

$$\alpha_4 = \frac{\delta}{\alpha} - 1, \alpha_5 = \frac{\Delta t}{2}\left(\frac{\delta}{\alpha} - 2\right), \alpha_6 = \Delta t(1-\delta), \alpha_7 = \delta \Delta t \tag{7}$$

Form the equivalent stiffness matrix $\bar{K}$:

$$\bar{K} = K + \alpha_0 M + \alpha_1 C \tag{8}$$

Perform a triangular decomposition on $\bar{K}$:

$$\bar{K} = LDL^T\big|_0 \tag{9}$$

2) Calculate the load, displacement, velocity and acceleration at $t+\Delta t$ moment for each integration step.

Load calculation:

$$\bar{P}_{t+\Delta t} = P_{t+\Delta t} + M\left(\alpha_0 \delta_t + \alpha_1 \dot{\delta}_t + \alpha_1 \ddot{\delta}_t\right) + C\left(\alpha_1 \delta_t + \alpha_4 \dot{\delta}_t + \alpha_5 \ddot{\delta}_t\right) \tag{10}$$

Displacement calculation:

$$LDL^T \delta_{t+\Delta t} = \bar{P}_{t+\Delta t} \tag{11}$$

Speed calculation:

$$\ddot{\delta}_{t+\Delta t} = \alpha_6\left(\delta_{t+\Delta t} + \delta_t\right) - \alpha_2 \dot{\delta}_t - \alpha_3 \ddot{\delta}_t \tag{12}$$

Acceleration calculation:

$$\dot{\delta}_{t+\Delta t} = \dot{\delta}_t + \alpha_6 \ddot{\delta}_t + \alpha_7 \ddot{\delta}_{t+\Delta t} \tag{13}$$

3 Seismic response model of subway station structure considering uniform damage

3.1 Overview of subway station structure

In this paper, finite element modeling is carried out on the A subway station structure. The station structure is 4.2m thick, 19m wide, 10.7m high, 4.72m high at the top level and 5.98m high at the bottom level, with concrete type C30 and reinforcement type HRB335. The top slab of the station is 0.8m thick, and the reinforcement rate is 1.21%. The middle slab is 0.6m thick with a reinforcement rate of 1.1%, the bottom slab is 1m thick with a reinforcement rate of 1.03%, and the side walls are 1.2m thick with a reinforcement rate of 0.5%. The cross-section of the central column of the station is a rectangle of 0.6×1 meters with a reinforcement rate of 2.01%, and the longitudinal spacing of the central column is 8 meters. Figure 1 shows the structural dimensions of the station and the distribution of soil layers.

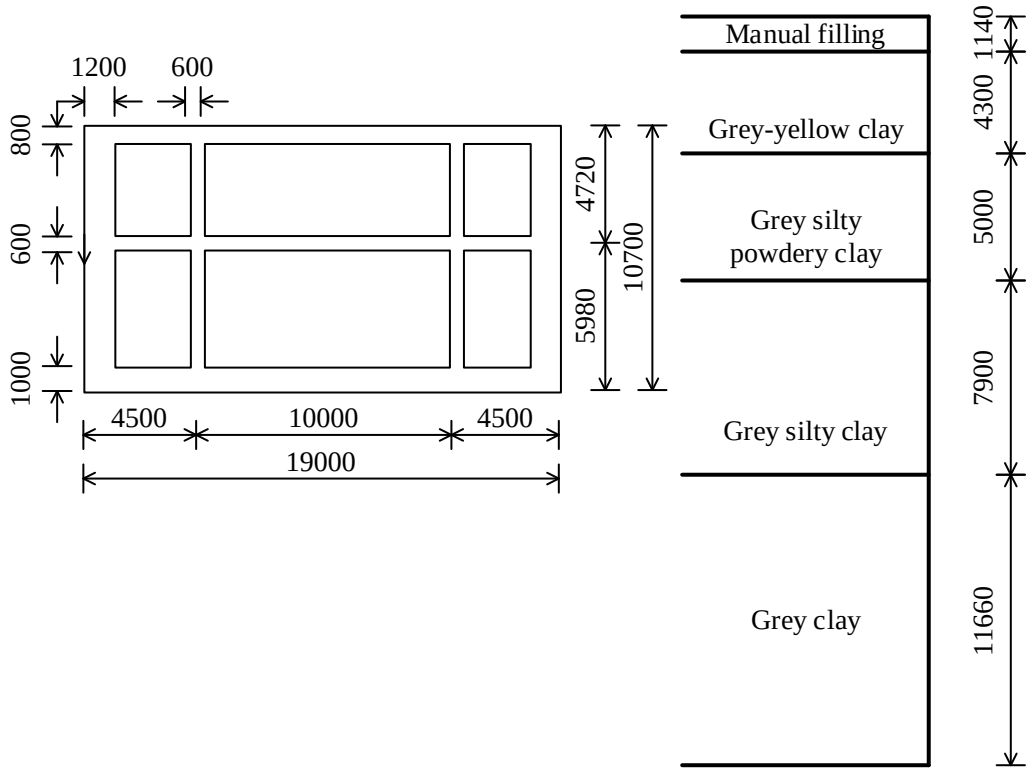

Figure 1. Station structure and distribution of soil layers

Table 1 shows the soil parameters.

Table 1. Physical parameters of the soil body

Soil layer	Thickness (m)	Gravity (kN/m^3)	Modulus of elasticity E (MPa)	Poisson's ratio V	Cohesion (kPa)	Internal friction angle ϕ (°)	Shear wave speed m/s
Artificial fill	1.14	18	167	0.4	20	33	180
Grayish yellow clay	43	18.2	226	0.38	30	32	210
Grey silty-powdered clay	5	17.5	194	036	25	31	200
Grey silty clay	7.9	17	270	0.35	25	31	240
Grey clay	11.66	17.6	316	0.3	25	31	260

Table 2 shows the basic parameters of concrete C30.

Table 2. Basic parameters of concrete C30

Modulus of elasticity (MPa)	Axial Compressive Strength Standard value (MPa)	Axial tensile strength standard value (MPa)	Density (Vm^3)	Poisson's ratio V
3×l0^4	20.1	2.01	2.4	0.2

Table 3 shows the basic parameters of reinforcing steel HRB335.

Table 3. Basic parameters of reinforcing steel HRB335

Modulus of elasticity (MPa)	Yield strength standard value (MPa)	Standard value of ultimate strength (MPa)	Density (t/m^3)	Poisson's ratio V
2×10^5	335	455	7.8	0.3

3.2 Material Ontology Model

3.2.1 Soil ontology Mohr-Coulomb plasticity model

1) Mohr-Coulomb strength theory

The Mohr-Coulomb plasticity model is based on the Mohr-Coulomb strength theory, assuming that the shear stress on the braking surface of the soil is affected by the normal stress on that surface and can be judged by the Mohr circle, and the expression of the shear strength of the soil is:

$$\tau = c + \sigma \tan \phi \tag{14}$$

Where τ is the maximum shear stress that any section of the soil can withstand. c is the cohesive force of the soil, σ is the positive stress perpendicular to the soil section, and ϕ is the angle of internal friction of the soil.

The Mohr-Coulomb model yield surface function is given by:

$$F = R_{mc} q - p \tan \phi - c = 0 \tag{15}$$

Where q is the Mises deflection stress, $q = \sqrt{3J_2}$. P is the equivalent compressive stress, and $P = -1/3 trac(\sigma)$. ϕ is the friction angle within the soil. R_{mc} is the shape parameter controlling the yield surface in the π plane.

2) Model plastic potential surface

The Mohr-Coulomb model uses the elliptic function proposed by Menetrey-Willam as the plastic potential surface of the model to avoid sharp corners in the analysis process. , whose expressions are:

$$G = \sqrt{\left(\varepsilon c|_0 \tan\psi\right)^2 + \left(R_{mw} q\right)^2} - p\tan\psi \tag{16}$$

Where ψ is the shear expansion angle of the soil. $c|_0$ is the cohesion of the soil, ε is the eccentricity on the meridian plane.

R_{mw} is the shape parameter controlling G in the π plane, which is calculated as:

$$R_{mw} = \frac{4\left(1-e^2\right)\cos^2\Theta + (2e-1)^2}{(2e-1)^2\cos\Theta + (2e-1)\sqrt{4\left(1-e^2\right)\cos^2\Theta + 5e^2 - 4e}} R_{mc}\left(\frac{\pi}{3}, \phi\right) \tag{17}$$

e is the eccentricity in the π plane that can change the shape of the $\Theta = 0 \sim \frac{\pi}{3}$ plastic potential surface in the π plane, which is calculated as:

$$e = \frac{3-\sin\varphi}{3+\sin\varphi} \tag{18}$$

The value of 1 ranges from 0.5 to e. At this time, the sharp angle of the plastic potential surface is tangential to yield in the π plane, and Figure 2 shows the corresponding plastic potential surface when e is at different values.

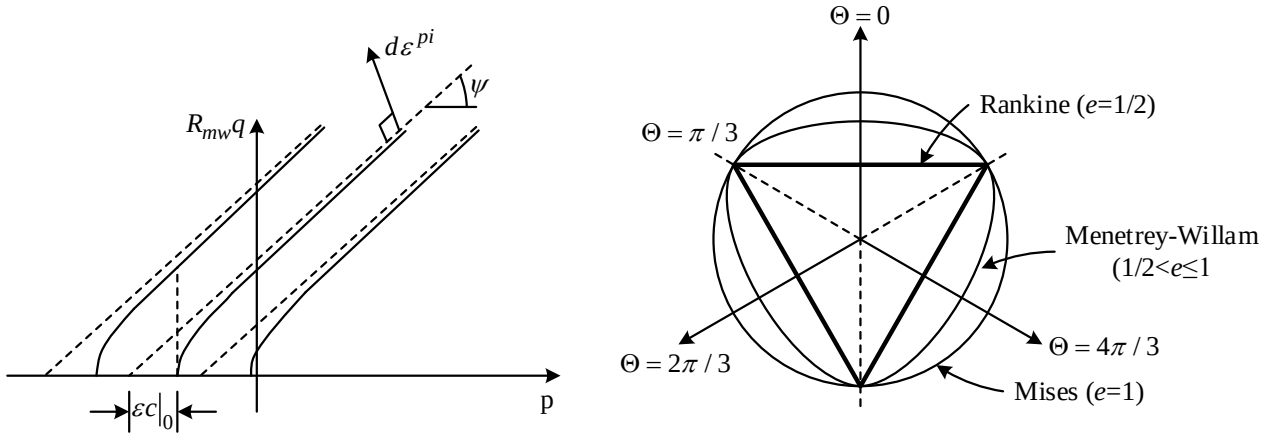

Figure 2. Plastic potential surface in Morh-Coulomb model

3.2.2 Concrete plastic damage

Assuming that the main causes of damage suffered by concrete are tensile cracking and compressive crushing, it can be used to simulate the mechanical behavior of concrete under monotonic loading, cyclic loading and dynamic loading.

1) Uniaxial tensile and compressive behavior

In concrete in uniaxial tension, when the stress is less than the failure stress σ_{t0}, the material is in the linear elastic stage concrete modulus of elasticity is expressed by E_0. When the stress reaches after σ_{t0} for unloading, at this time, the elastic modulus of concrete degenerates to $(1-d_t)E_0$, where d_t is the concrete damage factor in tension, taking the value of 0-1, 0 means no damage, 1 means completely damaged. Figure 3 shows the uniaxial tensile curve of concrete.

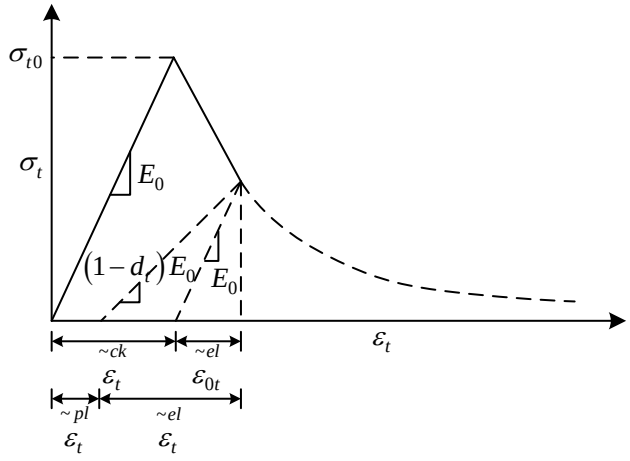

Figure 3. Uniaxial tension curve of concrete

When concrete is compressed in one axis, the material is linearly elastic when the stress is less than the yield stress σ_{c0}. When the stress is between yield σ_{c0} and the ultimate stress σ_{cu}, the concrete enters the strengthening phase. When the stress exceeds σ_{cu}, softening of the concrete occurs. When the stress reaches σ_{c0} for unloading, at this time, the elastic modulus of concrete degenerates to according to $(1-d_c)E_0$, where d_c is the damage factor of concrete under compression, taking a value of $0\sim1,0$ means no damage, 1 means complete damage. Figure 4 shows the uniaxial compressive curve of concrete.

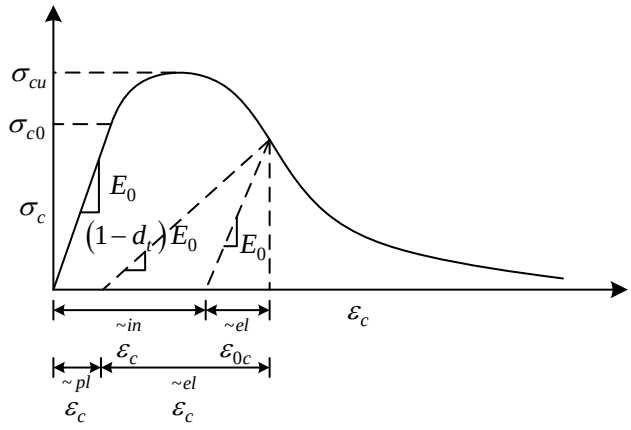

Figure 4. Uniaxial compression curve of concrete

The transformation relationship between plastic strain and actual strain leads to the following stress expression equation:

$$\sigma_t = (1-d_t)E_0\left(\varepsilon_t - \tilde{\varepsilon}_t^{pl}\right) \tag{19}$$

$$\sigma_c = (1-d_c)E_0\left(\varepsilon_c - \tilde{\varepsilon}_c^{pl}\right) \tag{20}$$

2) Uniaxial cyclic loading

Concrete under uniaxial cyclic loading, cracking and crack closure will occur, and the mechanical mechanism of concrete is more complex at this time. Under unidirectional loading, cracks begin to appear in the concrete, and its stiffness decreases. When reverse loading, the cracks close and the material stiffness is restored. In the CDP model, the damage factor d is used to represent this mechanism of material stiffness degradation so that the relationship between the modulus of elasticity E and the initial modulus of elasticity E_0 after material stiffness degradation can be expressed as:

$$E = (1-d)E_0 \tag{21}$$

Damage factor d is jointly determined by tensile damage factor d_t and compressive damage factor d_c. Under uniaxial cyclic loading, the expressions are:

$$(1-d) = (1-s_t d_c)(1-s_c d_t) \tag{22}$$

In the above equation, s_t and s_c are the stress state functions related to the opposite direction of stress, respectively, which are defined as:

$$\begin{aligned} s_t &= 1 - w_t r^*(\sigma_{11}) \qquad 0 \le w_t \le 1 \\ s_c &= 1 - w_c\left(1 - r^*(\sigma_{11})\right) \quad 0 \le w_c \le 1 \end{aligned} \tag{23}$$

Among them:

$$r^*(\sigma_{11}) = H(\sigma_{11}) = \begin{cases} 1 & \sigma_{11} > 0 \\ 0 & \sigma_{11} < 0 \end{cases} \tag{24}$$

Figure 5 shows the schematic diagram of the stiffness recovery of concrete under cyclic loading. When the material is in tension, the OA section is in the linear elastic stage, and the modulus of elasticity of the material is E_0. After the peak tensile stress A point, the concrete starts to crack, and after loading to point B, it starts to unload, and the modulus of elasticity of the concrete is $(1-d_t)E_0$. When the material is loaded in the opposite direction, if the recovery factor of compressive stiffness is $w_c = 1$, the compressive stiffness is fully recovered, and the modulus of elasticity of the concrete is still E_0 at this time, and the loading path CDN is continued to reach the point N for unloading, and the modulus of elasticity of the concrete is $(1-d_c)E_0$ at this time. When the load is reversed again, if the tensile stiffness recovery factor is $w_t = 0$, the tensile stiffness is damaged and the loading path changes along MG.

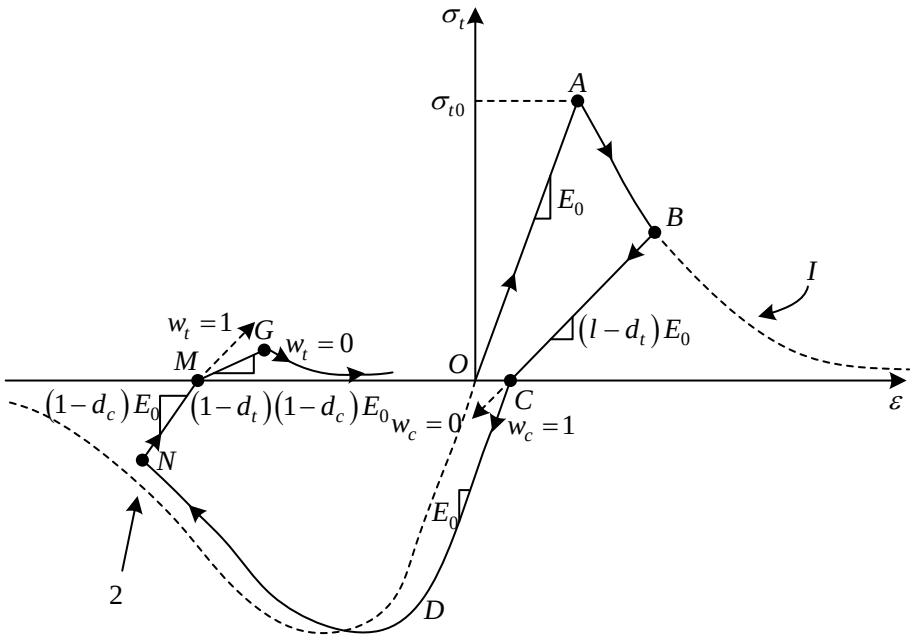

Figure 5. CDP model stiffness recovery by reciprocal loading

3.2.3 Concrete stress-strain relationship curve

The uniaxial tensile and compressive-stress-strain curves for concrete are as follows.

1) When concrete is subjected to uniaxial tension:

$$\sigma=(1-d_t)E_c\varepsilon \tag{25}$$

$$d_t=\begin{cases}1-\rho_t\left[1.2-0.2x^5\right] & (x\le 1)\\ 1-\dfrac{\rho_t}{\alpha_t(x-1)^{1.7}+x} & (x>1)\end{cases} \tag{26}$$

$$x=\frac{\varepsilon}{\varepsilon_{t,r}} \tag{27}$$

$$\rho_t=\frac{f_{t,r}}{E_c\varepsilon_{t,r}} \tag{28}$$

2) Concrete uniaxially compressed:

$$\sigma=(1-d_c)E_c\varepsilon \tag{29}$$

$$d_c = \begin{cases} 1-\dfrac{\rho_c n}{n-1+x^n} & (x \le 1) \\ 1-\dfrac{\rho_c}{\alpha_c (x-1)^2 + x} & (x > 1) \end{cases} \tag{30}$$

$$\rho_c = \frac{f_{c,r}}{E_c \varepsilon_{c,r}} \tag{31}$$

$$n = \frac{E_c \varepsilon_{c,r}}{E_c \varepsilon_{c,r} - f_{c,r}} \tag{32}$$

$$x = \frac{\varepsilon}{\varepsilon_{c,r}} \tag{33}$$

3.2.4 Sidoroff energy equivalence principle

Sidoroff's energy equivalence principle, whereby stresses produce the same form of residual elastic energy in a damaged material as in a nondamaged material, allows the replacement of stress σ with equivalent force $\bar{\sigma}$ or the conversion of modulus of elasticity E_0 to modulus of elasticity E_d at the time of damage.

Residual energy of elasticity in undamaged materials:

$$W_0^{\varepsilon} = \frac{\sigma^2}{2E_0} \tag{34}$$

Residual elastic energy of lossy materials:

$$W_D^{\varepsilon} = \frac{\bar{\sigma}^2}{2E_0} = \frac{\sigma^2}{2E_d} \tag{35}$$

$$\bar{\sigma} = \frac{\sigma}{1-D} \tag{36}$$

Combining equations (34), (35) and (36) yields:

$$E_d = \left(1-D_K\right)^2 E_0 (k=c,t) \tag{37}$$

Further obtained:

$$\sigma_K = \left(1-D_K\right)^2 E_0 \varepsilon_K (k=c,t) \tag{38}$$

Uniaxial stress-strain relationships for concrete:

$$\sigma_k = \left(1-d_k\right) E_0 \varepsilon_k (k=c,t) \tag{39}$$

Where parameter d_k is the damage evolution parameter, and the joint (38)(39) equation yields:

$$D_k = 1 - \sqrt{1 - d_k}\,(k = c, t) \tag{40}$$

The relationship between the concrete damage factor D_k and the concrete damage evolution parameter d_k can be obtained from equation (40).

4 Seismic performance analysis of underground frame structure of subway station

4.1 Effect of station structure form on displacement

In this paper, EL-Centro wave is used for the simulation analysis, and horizontal seismic excitation is applied to the station model of rectangular structure form and the station model of arched structure form, respectively. Table 4 shows the test loading conditions.

Table 4. Test loading conditions

Serial number	Condition Number	Seismic wave	Structure	
			X	Z
1	EL-1	E1 Centro Wave	0.036	-
2	EL-2	E1 Centro Wave	0.065	-
3	EL-3	E1 Centro Wave	0.022	-

The EL-3 and EL-2 operating conditions are selected to compare the relative displacements of the top and bottom of the arched station and rectangular structure station models. According to the numerical simulation results, the displacement responses of the rectangular station model and the arched station model gradually decrease from the top of the model to the bottom of the model. With the increase of the peak input acceleration, the displacement response of the two station models shows a pattern of increasing with the increase of seismic excitation. In the EL-3 condition, the displacement of S1 measurement point of the arched station is 3.932 mm, and the relative displacement of S1 measurement point of the rectangular station is 7.503 mm. In the EL-2 condition, the displacement of S3 measurement point of the arched station is 3.143 mm, and the first pair displacement of S3 measurement point of the rectangular station is 5.695 mm. The peak relative displacements of the measurement points and the bottom measurement points are relatively small. Table 5 shows the peak relative displacement of each measurement point and the bottom measurement point.

Table 5. Relative displacement of each measurement point

Measurement points	S1	S2	S3	S4	S5	S6	S7
Arched station-EL-3 (mm)	3.932	3.523	3.143	2.745	2.245	1.755	0
Arched station-EL-2 (mm)	1.691	1.594	1.544	1.416	1.303	1.183	0
Rectangular station-EL-3 (mm)	7.503	6.404	5.695	4.594	3.525	2. 058	0
Rectangular station-EL-2 (mm)	3.075	2.729	2.494	2.144	1.817	1.358	0

4.2 Effect of concrete strength on the dynamic response of underground structures in subway stations

To study the effect of concrete material strength on the seismic response of subway underground

structure, it is assumed that the model soil layer is a single homogeneous soil layer, and the soil is taken as plastic loess, the density of structural model material is changed, and the finite element model of the underground structure and other parameters of material and burial depth is kept constant. The acceleration value of 0.1g of E1 Centro wave ground vibration is input at the bottom of the model, and the difference of relative displacement of the top and bottom plates of the station structure and the change of internal structural force is considered.

Fig. 6 Relative displacement of side walls of station structure. Figure 7: Relative horizontal displacement time curve of the top and bottom slab of the station structure. 0.3 times the concrete strength, the relative displacement is 1.5 mm for a sidewall height of 3 m. 0.6 times the concrete strength, the relative displacement is 1.4 mm for a sidewall height of 3 m. The relative displacement of the original concrete strength is 1.2 mm for a sidewall height of 3 m. The relative displacement of the station structure remains basically the same for different concrete strengths. The relative displacement of the station structure remains the same for different concrete strengths. The changing pattern of the time course curve of the top and bottom slab of the station with different concrete strengths is consistent, and the amplitude of the time course curve remains the same.

Table 6 shows the values of internal forces in each section of the station structure. 2042.68 KN for the cross-sectional axial force of 0.3 times the concrete strength in section A1. 2053.84 KN for the cross-sectional axial force of 0.6 times the concrete strength in section A1. 989.78 KN*m for the cross-sectional bending moment of 0.3 times the concrete strength in section A1. 991.76 KN*m for the cross-sectional bending moment of 0.6 times the concrete strength in section A1. The effect of concrete strength on the internal force of the station structure under earthquake load is basically negligible. The variation of concrete strength has a limited effect on the magnitude of horizontal displacement and the time course curve of the top and bottom slab displacement of the underground structure of the subway station. The effect on the internal forces of the main observation surfaces of the station structure is basically negligible.

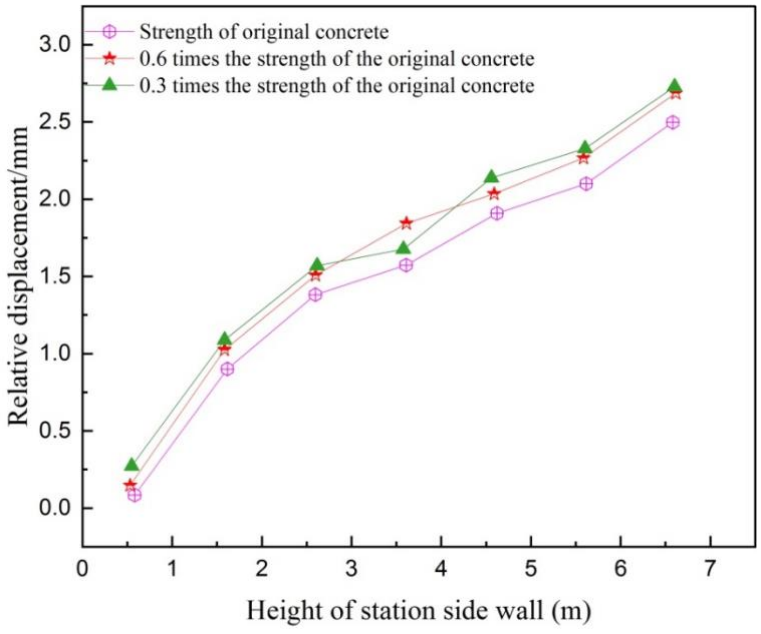

Figure 6. Relative displacement of station structure side walls

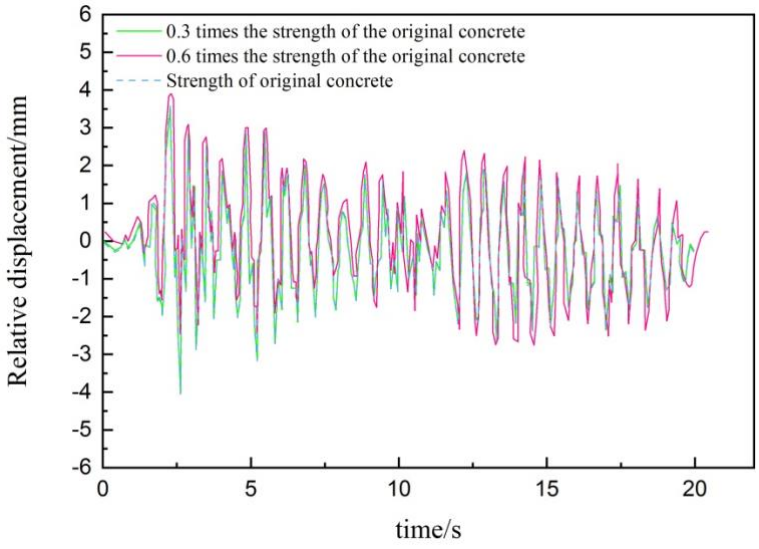

Figure 7. Time course curve of relative horizontal displacement of top and bottom plate

Table 6. The station structure each section internal force value

Cross-section number	Cross-sectional axial force (KN)			Cross-sectional bending moment (KN*m)		
	0.3 times	0.6 times	The original concrete The intensity of soil	0.3 times	0.6 times	The original strength of concrete
A1	2042.68	2053.84	2070.76	989.78	991.76	986.51
A2	1852.65	1660.40	1843.38	992.75	993.16	993.79
A3	512.72	515.19	503.61	1549.11	1553.74	1558.07
A4	523.35	528.51	531.71	1628.38	1630.98	1631.65
AS	4673.47	4438.92	4976.74	427.59	429.71	433.09
A6	1504.34	1508.65	1545.56	1218.51	1220.67	1524.45
A7	1727.47	1736.47	1739.44	1467.77	1304.38	1667.56
A8	1536.52	1567.88	1571.94	1398.87	1400.43	1401.14
A9	4865.35	4877.26	4965.72	466.75	445.82	480.61
A10	1538.44	1546.42	1551.56	1181.57	1182.99	1183.59

4.3 Effect of soil stiffness on the dynamic response of underground structures in subway stations

To study the effect of dynamic shear modulus Gmax on the seismic response of subway underground structure, it is assumed that the model soil layer is a single homogeneous soil layer, other parameters of the soil are kept constant, the soil is taken as plastic loess, the finite element model of the underground structure and material parameters and burial depth is kept constant. The shear modulus Gmax=80Mpa, Gmax=100MPa, Gmax=150MPa and Gmax=200MPa of the three soils are taken respectively, and the E1-Centro ground shaking with acceleration value of 0.1g is input at the bottom of the model to consider the difference of structural displacement of the station under the above three cases.

Figure 8 shows the time course of relative horizontal displacement of the station structure sidewall under the three cases of the maximum dynamic shear modulus of soil. Figure 9 shows the relative horizontal displacement curves of the top and bottom slabs of the station structure for three types of

soil masses with maximum dynamic shear modulus. With the increase of the maximum dynamic shear modulus of soil, the peak value of the time course curve of the relative horizontal displacement of the top and bottom of the station decreases, and the maximum value of the relative horizontal displacement of the top and bottom of the sidewall also has the same pattern. In the weak site where the maximum dynamic shear modulus of the soil is small, the deformation of the underground structure is larger compared to that of the underground structure, which causes damage to the underground structure.

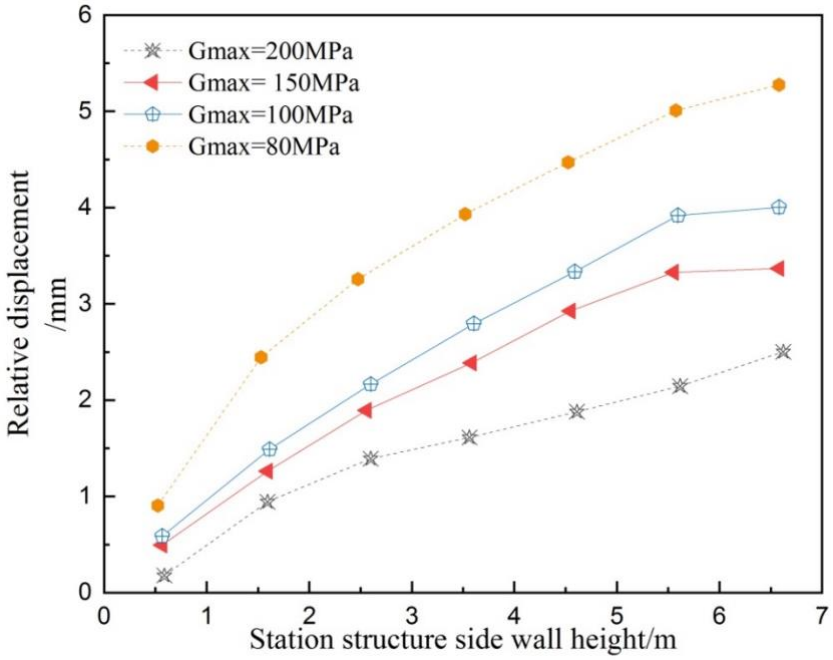

Figure 8. Relative displacement of station structure side walls

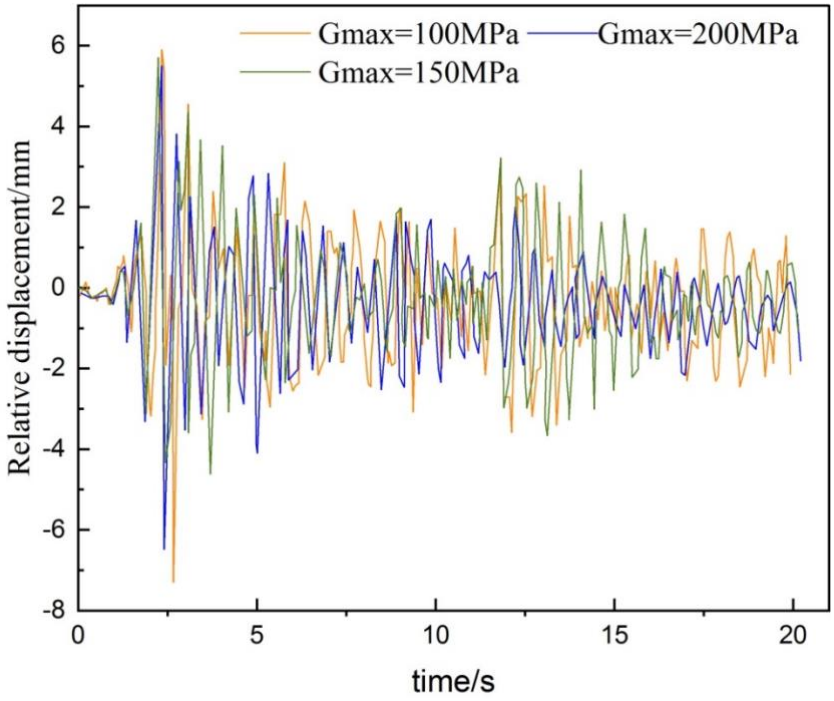

Figure 9. Time course curve of relative horizontal displacement of top and bottom plate

5 Conclusion

In this paper, the finite element model of the subway station structure is established based on the dynamic finite element theory, and the material ontological model is studied to determine the calculation of the stress-strain relationship and the damage calculation method for various materials, and the influence of structural form on displacement and the influence of concrete strength and soil stiffness on the dynamic response of the underground structure of the subway station is studied. The following conclusions are drawn:

Under EL-2 working conditions, the displacement of S3 measurement point of the arch station is 3.143, and the first pair displacement of S3 measurement point of the rectangular station is 5.695. The relative displacement of different measurement points of its station model and the peak of the bottom measurement point are relatively small under the same seismic action.

The shear modulus of soil with Gmax=80Mpa has a relative displacement of 3.5 mm for a sidewall height of 3 m. The shear modulus of soil with Gmax=200Mpa has a relative displacement of 2.3 mm less than that of soil with Gmax=80Mpa for the same condition. With the increase of the maximum dynamic shear modulus of soil, the peak of the relative horizontal displacement time curve of the top and bottom slab of the station decreases.

The relative displacement of 0.6 times concrete strength is 0.1 mm less than that of 0.3 times concrete strength for a sidewall height of 3 m. The effect of concrete strength on the internal force, horizontal displacement, and internal force of the observation surface of the station structure under seismic loading is basically negligible.

References

[1] Wenting, Chen, & Qingjun. (2018). Seismic performance and failure mechanism of a subway station based on nonlinear finite element analysis. KSCE journal of civil engineering.

[2] Du, X., Liu, H., Xu, C., Jin, L., & Li, S. (2018). Experimental study on seismic performance of precast column in assembled monolithic subway station under different axial compression ratio. Jianzhu Jiegou Xuebao/Journal of Building Structures, 39(11), 11-19.

[3] Xue-Jian, W., Hai-Yang, Z., Guo-Xing, C., & Rui, W. (2017). Effect of diaphragm wall on earthquake responses of an underground subway station. Chinese Journal of Geotechnical Engineering.

[4] Tang, B., Li, X., Chen, S., Zhuang, H., & Chen, H. P. (2020). Investigations of seismic response to an irregular-section subway station structure located in a soft clay site. Engineering Structures, 217, 110799.

[5] Chen, Z., & Zhou, Y. (2019). Seismic performance of framed underground structures with self-centering energy-dissipation column base. Advances in Structural Engineering, 22(13), 2809-2822.

[6] Huang, P., Ge, H., & Chen, Z. (2022). Rapid seismic damage evaluation of subway stations using machine learning techniques. International Journal of Computational Methods.

[7] Liu, H., Wang, Z., Du, X., & Shen, G. (2021). The seismic behaviour of precast concrete interior joints with different connection methods in assembled monolithic subway station. Engineering Structures, 232(2), 111799.

[8] Yu, Z., & Zhang, H. (2019). Seismic characteristics and design method for cross transfer subway stations. Journal of Southeast University (Natural Science Edition).

[9] Huang, P., & Chen, Z. (2021). Deep learning for nonlinear seismic responses prediction of subway station. Engineering Structures, 244(5), 112735.

[10] Liu, Z. Q., Chen, Z. Y., & Zhao, H. (2020). Characteristics of earthquake input energy of a subway station structure based on probability density evolution method. International Journal of Computational Methods.

[11] Chen, Z., Huang, P., & Chen, W. (2021). Seismic response characteristics of multi-story subway station through shaking table test: Advances in Structural Engineering, 24(10), 2185-2200.

[12] Hou, C., Xiaoguang, Yan, G., & Jie, H. (2021). Shaking table test on the seismic response of a frame-type subway station in composite soil. International journal of geomechanics.

[13] Lu, D., Li, Q., Du, X., & Wu, C. (2019). Research on seismic performance of subway station based on failure model control. Yantu Gongcheng Xuebao/Chinese Journal of Geotechnical Engineering, 41(8), 1400-1407.

[14] Miao, P., & Cui, W. J. (2018). Study on seismic dynamic response of shallow-buried subway station structure and ancillary facilities. Civil Engineering Journal, 4(12), 2853.

[15] Liu, G., & Hou, Z. (2020). Adaptive iterative learning control for subway trains using multiple-point-mass dynamic model under speed constraint. IEEE Transactions on Intelligent Transportation Systems, PP (99), 1-13.

[16] Chen, C. (2019). Seismic response and damage of underground subway station in a slightly sloping liquefiable site. Bulletin of earthquake engineering, 17(11).

[17] Liang, J. W., & Zhu, J. (2018). Fem-ibem coupling method for nonlinear seismic response analysis of underground structures in water-saturated soft soils. Yantu Gongcheng Xuebao/Chinese Journal of Geotechnical Engineering, 40(11), 1977-1987.

[18] Li, W., & Chen, Q. (2020). Effect of vertical ground motions and overburden depth on the seismic responses of large underground structures. Engineering Structures, 205(Feb.15), 110073.1-110073.18.

About the Author

Hongshuo Sun was born in Shijiazhuang, Hebei, PR China, in 1986. He received his master's degree from Shijiazhuang Tiedao University, PR China. Now, he works at Zhengzhou Railway Vocational and Technical College. His main research area is Tunnel works.

Hongtao Dai was born in Zhengzhou, Henan, PR China, in 1986. He received his master's degree from the South China University of Technology, PR China. Now, he works at Zhengzhou Railway Vocational and Technical College. His main research area is seismic resistance of building structures.